Revista Mexicana de Astronomía y Astrofísica, **47**, 113–125 (2011)

MASS AND METAL EJECTION EFFICIENCY IN DISK GALAXIES DRIVEN BY YOUNG STELLAR CLUSTERS OF NUCLEAR STARBURST

A. Rodríguez-González,[1] A. Esquivel,[1] A. C. Raga,[1] and P. Colín[2]

Received 2010 August 26; accepted 2011 January 31

RESUMEN

Presentamos las eficiencias de pérdida de masa y metales obtenidas de modelos numéricos de vientos galácticos empujados por la energía depositada en brotes de formación estelar nucleares. Los brotes de formación estelar contienen cúmulos estelares jóvenes los cuales inyectan la energía suficiente para empujar parte del medio interestelar fuera de las galaxias. En algunos casos los vientos galácticos contienen una importante parte de los metales producidos por las nuevas generaciones estelares. Para estudiar las eficiencias de pérdida de masa y metales hemos desarrollado simulaciones numéricas 3D *N-Cuerpos/Smooth Particle Hydrodynamics* de vientos galácticos para los casos: adiabáticos y con pérdidas radiativas. Los modelos numéricos cubren una amplio intervalo de masas de los brotes de formación estelar (de $\sim 10^2$ a $\sim 10^7$ $M_\odot$) y de masas en las galaxias anfitrionas (de $\sim 6\times 10^6$ a $\sim 10^{11}$ $M_\odot$). Las regiones de formación estelar concentradas en el centro del potencial son una maquinaria importante para la pérdida y redistribución de masa y metales en este tipo de galaxias.

ABSTRACT

We present results from models of galactic winds driven by energy injected by nuclear starbursts. The total energy of the starburst is provided by young central stellar clusters and parts of the galactic interstellar medium are pushed out as part of the galactic wind (in some cases the galactic wind contains an important part of the metals produced in the new generation of stars). We have performed adiabatic and radiative 3D N-Body/Smooth Particle Hydrodynamics simulations of galactic winds using the GADGET-2 code. The numerical models cover a wide range of starburst (from $\sim 10^2$ to $\sim 10^7$ $M_\odot$) and galactic gas masses (from $\sim 6 \times 10^6$ to $\sim 10^{11}$ $M_\odot$). The concentrated central starburst regions are an efficient engine for producing the mass and metal loss in galaxies, and also for driving the metal redistribution in galaxies.

Key Words: galaxies: starburst — galaxies: star clusters: general — ISM: general — stars: winds, outflows

© Copyright 2011: Instituto de Astronomía, Universidad Nacional Autónoma de México

1. INTRODUCTION

A great amount of evidence, both observational and theoretical, indicates that galactic winds (GWs) are a necessary and very important ingredient of the evolution of galaxies and the inter-galactic medium. Their presence can explain, among other things, the very low metallicities found in dwarf galaxies, and the abundance of metals observed in the intracluster medium. Such outflows have been observed in galaxies of a variety of masses and at different redshifts (e.g., Martin 1999; Pettini et al. 2001; Veilleux, Cecil, & Bland-Hawthorn 2005). At the same time, different analytical and numerical models have been put forward to explain these outflows (e.g., Chevalier & Clegg 1985; Tomisaka & Ikeuchi 1988; Heckman, Armus, & Miley 1990; De Young & Heckman 1994; MacLow & Ferrara 1999; Strickland & Stevens 2000; Cantó, Raga, & Rodríguez 2000; Tenorio-Tagle, Silich, & Muñoz-Tuñón 2003; Fujita et al. 2004; Cooper et al. 2008; Fujita et al. 2009; Rodríguez-González, Raga, & Cantó 2009).

[1]Instituto de Ciencias Nucleares, Universidad Nacional Autónoma de México, Mexico.

[2]Centro de Radioastronomía y Astrofísica, Universidad Nacional Autónoma de México, Mexico.

© Copyright 2011: Instituto de Astronomía, Universidad Nacional Autónoma de México

Long ago, Lynds & Sandage (1963) found a large outflow in M82 and gave the first definition of a starburst (SB). They proposed that material was ejected from the nuclear regions as a consequence of a series of SN explosions. Since then, galaxies with concentrated central starbursts (M82, NGC 253, NGC 1569, to name a few) have been used to study the GW phenomenon.

Tenorio-Tagle & Muñoz-Tuñón (1998) showed the importance of the galactic potential component due to the cold dark matter halo in realistic models of GW, and concluded that the fate of the stellar wind and SNe material depends on the galactic properties and on the total energy injected by the SB. They showed that dwarf galaxies with an interstellar medium (ISM) with masses of the order of $10^9\ M_\odot$, retain their metals unless they undergo an extreme burst of star formation, much larger than those presently observed. On the other hand, MacLow & Ferrara (1999) explored both, analytically and numerically, the effects of stellar winds and SN explosions, in SBs with mechanical luminosities in the $\sim 10^{37} - 10^{39}$ erg s^{-1} range on the ISM of dwarf galaxies with gas masses in the $\sim 10^6$ to $10^9\ M_\odot$ range. They distinguished between two possibilities of gas ejection: (a) A "blowout", which requires material be accelerated above the escape speed at a distance of about three times the scale height. (b) A "blow-away", in which virtually all the ISM is accelerated and lost to the galaxy. The blowout would happen preferably for flatter galaxies; rounder galaxies are more likely to be completely disrupted (blow-away) if enough energy is injected. Their conclusion was that dwarf galaxies in that mass range undergo blowout for moderate-to-high luminosity starbursts values ($L \sim 10^{38} - 10^{39}$ erg s^{-1}), whereas for galaxies with gas masses $M_g > 10^8\ M_\odot$ and mechanical luminosity $L \sim 10^{37}$ erg s^{-1} the blowout was inhibited. They also found that in the lowest mass objects, blow-away occurs virtually independently of L.

Many authors have shown that in the nearest starburst galaxies GWs could form through the collective effect of many individual stellar cluster winds, which in turn are formed by the collective effect of many individual stellar winds. Perhaps the best studied starburst galaxy is M82, which has an extended, biconical filamentary structure in the optical (Shopbell & Bland-Hawthorn 1998; Ohyama et al. 2002). In M82, the super stellar clusters (SSCs) have Hα luminosities in the $(0.01-23)\times 10^{38}$ erg s^{-1} range (Melo et al. 2005). These authors compiled a catalog of 197 SSCs in M82 and 48 SSCs in NGC 253 (Melo 2005), with masses in the $10^4 < M/M_\odot < 10^6$ range (more recently, additional young star clusters in M82 have been reported by Smith et al. 2007 and Westmoquette et al. 2007). Other examples are NGC 1569 (Anders et al. 2004; Westmoquette, Smith, & Gallagher 2008) and M83 (Harris et al. 2001), with SSCs densities and masses similar to those of M82. Such an exceptional density of massive clusters (i.e. $\sim$620 kpc^{-2}, see also Anders et al. 2004; Melo et al. 2005; Melo 2005) is the best scenario to study powerful GWs driven by SSC winds originated in nuclear starburst regions.

Yet another interesting effect is when the material ejected from the SSCs winds does not abandon the galaxy. Tenorio-Tagle (1996) explored the effect of a non-uniform interstellar medium (density and temperature) in the cooling efficiencies within the giant cavities. In high density regions the cooling would be more effective and would produce a series of metal-rich cloudlets. Such cloudlets would fall back to the disk and produce local enhancements of metallicity. However, Recchi, Matteucci, & D'Ercole (2001) and Recchi et al. (2008) presented arguments against this scenario, pointing out that thermal conduction and hydrodynamical drag are likely to disrupt the condensations before they reach the disk, and thus the metals would be spread more or less uniformly throughout the galaxy.

In the present paper we study the effects of young stellar clusters in the nuclear starburst (SB) region on the ISM of dwarf disk-galaxies. In particular, we calculate the amount of enhanced metallicity material that will end up in the intergalactic medium (IGM) and/or in the outer regions of the galactic disk. The paper is organized as follows: in § 2 we describe the ingredients of the galactic models that we use. In § 3 we discuss the possible fate of the mass and metals in such galaxies. In § 4 we describe a series of 3D simulations of the interaction of SSCs with the galactic ISM. The results are presented in § 5, and our conclusions in § 6.

2. GALACTIC MODEL INGREDIENTS

Each galaxy in our study consists of a dark matter halo, and a rotationally supported disk of gas and stars. The models are constructed following the approach described in Springel, Di Matteo, & Hernquist (2005, see also Hernquist 1993 and Springel 2000). A near-equilibrium galaxy model is constructed, with a dark matter halo that follows a Hernquist (1990) profile, and a disk with exponential surface gas density. Then, using an iterative procedure, the vertical gas profile is determined self-

© Copyright 2011: Instituto de Astronomía, Universidad Nacional Autónoma de México

consistently for a particular effective equation of state.

2.1. *The halos*

We modeled the dark matter mass distribution with the Hernquist profile (Hernquist 1990),

$$\rho_h(r) = \frac{M_{\rm dm}}{2\pi} \frac{a}{r(r+a)^3}\,, \tag{1}$$

where r is the radial distance, and $M_{\rm dm}$ is the dark matter mass. Two remarks can be made about the shape of this profile: (i) In the inner parts of the galaxy it agrees with the profile given by the Navarro, Frenk, & White (1996, henceforth NFW) fitting formula. (ii) Its faster than r^{-3} decline causes the total mass to converge, allowing the construction of isolated halos without the need of an *ad hoc* truncation. The a parameter is related to the scale radius r_s of the NFW profile by:

$$a = r_s\sqrt{2[\ln(1+c) - c/(1+c)]}\,, \tag{2}$$

where $c = r_{200}/r_s$ is the concentration parameter, r_{200} is the radius at which the enclosed dark matter mean density is 200 times the critical value (where the critical density is $\rho_{\rm crit} = 3H^2/8\pi G$). We have set $c = 9$.

2.2. *The disk*

We modeled gas and star disk components with an exponential surface density profile (in the radial direction of the galactic disk, R) the scale of length being R_0,

$$\Sigma_g(R) = \frac{M_g}{2\pi R_0^2}\exp(-R/R_0)\,, \tag{3}$$

$$\Sigma_*(R) = \frac{M_*}{2\pi R_0^2}\exp(-R/R_0)\,, \tag{4}$$

so that the total mass of the disk is $M_d = (M_g + M_*) = m_d M_{\rm tot}$, where m_d is a dimensionless parameter (fixed in this work to $m_d = 0.041$), and $M_{\rm tot}$ is the total mass of the galaxy, incuding the dark matter halo (i.e. $M_{\rm tot} = M_d + M_h$, where M_h is the mass of the halo). The vertical mass distribution of the stars in the disk is specified by the profile of an isothermal slab with a constant scale height H. The 3D stellar density in the disk is hence given by,

$$\rho_*(R,z) = \frac{M_*}{4\pi\, H\, R_0^2}\,{\rm sech}^2\left(\frac{z}{2H}\right)\exp\left(-\frac{R}{R_0}\right)\,. \tag{5}$$

In all models, H/R_0 was fixed to 0.2 whereas the relative content of gas in the disk (the rest of the disk mass is in stars) was set to 0.35. On the other hand, the disk spin fraction (the fraction of the total angular momentum in the disk), was set, as is customary, to the value of m_d. These values are typical of low-mass galaxies (e.g., Springel et al. 2005).

2.3. *Vertical structure of the gas disk*

The vertical structure of the disk at the beginning of the simulation is computed self-consistently with the halo and stellar disk components as follows. At $t = 0$ the gaseous disk has uniform temperature (fixed to 1000 K). Consider the vertical structure of the gas disk in hydrostatic equilibrium:

$$\frac{\partial\rho_g}{\partial z} = -\frac{\rho_g^2}{\gamma P}\frac{\partial\Phi_T}{\partial z}\,, \tag{6}$$

where, $\Phi_T = \Phi_h + \Phi_d$ is the total gravitational potential (Φ_h and Φ_d are the halo and disk gravitational potentials, respectively). For a given Φ_T, the solution of this equation is constrained by the condition

$$\Sigma_g(R) = \int \rho_g(R,z)dz\,, \tag{7}$$

where $\Sigma_g(R)$ is the gaseous surface mass density (see also equation 3). One can obtain the vertical distribution by integrating equation (6), with a central density value at the midplane ($z = 0$) and an effective equation of state of the form $P = P(\rho)$, see Springel et al. (2005). The starting value for the density is guessed, then adjusted in an iterative scheme until the desired surface density (equation 3) is recovered. This process is repeated for different radii to obtain an axisymmetric gas density distribution.

2.3.1. *Cooling*

For the non-adiabatic cases, we adopt the cooling functions computed in collisional ionization equilibrium (CIE) by Sutherland & Dopita (1993). The energy loss per unit mass of the gas is given by,

$$\left(\frac{du}{dt}\right)_{\rm cool} = -\frac{\Lambda_{\rm net}(\rho,T)}{\rho}\,. \tag{8}$$

We must note that the cooling function we used in our models assumes solar abundances. However, the kind of galaxies treated in this paper should be less metallic and thus the cooling should be lower. For the less metallic galaxies the results would be shifted from our radiative models to the adiabatic ones.

© Copyright 2011: Instituto de Astronomía, Universidad Nacional Autónoma de México

3. THE FATE OF THE GAS INJECTED BY YOUNG STELLAR CLUSTERS

Depending on the total amount of kinetic energy injected by the SSCs two outcomes are possible: if the kinetic energy is larger than the gravitational potential of the galaxy, all material will escape and become part of the IGM; otherwise, the gas will return to the disk. If the material returns and reincorporates to the galaxy two things can happen: it can fall back close to the galactic center or far from it. Considering that GWs are confined to a cone, material that does not reach a high altitude will fall close to the galactic center, while gas that reaches a high altitude can fall back at large galactocentric radii.

3.1. *Mass loss measures*

In order to quantify the mass loss in numerical models one has to determine which material will be considered lost to the IGM. A natural estimation can be derived by comparing the velocity of a parcel of gas and the escape velocity at its current position. This has been done, for instance, in previous work by MacLow & Ferrara (1999) and D'Ercole & Brighenti (1999). This work, however, used Eulerian codes in which material that leaves the computational domain cannot be further analyzed, and therefore was automatically considered unbound. In reality, some of this material would return to the galaxy. Our models, that use the SPH (Smooth Particle Hydrodynamics) integration scheme, are not limited by the extent of the computational domain; thus, they were able to trace all the material for the duration of the simulation. We will consider the following more stringent criterion: only material that has left a cylindrical region of $R_{\rm max} = 20$ kpc and $|z_{\rm max}| = 20$ kpc (see also D'Ercole & Brighenti 1999) *and* has a velocity larger than the escape velocity at its current position will be considered effectively lost.

Mass loss in our models is thus carried out by first computing the total mass of unbound (ejected from the galaxy) gas $M_{\rm ej}$. To do this, we consider the total galaxy gravitational potential given by,

$$\Phi_T(r) = \Phi_h(r) + \Phi_d(r)\,, \tag{9}$$

where r is the distance to the center, and Φ_h and Φ_d are the dark matter halo and disk components, respectively. Gas particles outside the cilinder with velocity larger than the escape velocity

$$v_{\rm esc} = \sqrt{-2\Phi_T(r)} \tag{10}$$

are considered to be unbound. We define a 'total mass ejection efficiency' as the ratio of the mass ejected (unbound) to the total gas mass,

$$\xi_m \equiv \frac{M_{\rm ej}}{M_g}\,. \tag{11}$$

The mass ejection efficiency has two limiting cases: $\xi_m \rightarrow 0$ when all the galactic ISM is bound, and $\xi_m \rightarrow 1$ when all the galactic gas is expelled from the galaxy.

One can also define a "metal ejection efficiency" as

$$\xi_z \equiv \frac{M_{c,\rm ej}}{M_c}, \tag{12}$$

where M_c is the total mass injected by the SSCs, and $M_{c,\rm ej}$ the mass, also originated in the SSCs, that is unbound. The mass injected by a star cluster contains the metals produced in the lifetime of the massive stars, $t\sim$40 Myr. For that time-span, using the metal yields calculated by Meynet & Maeder (2002), Tenorio-Tagle et al. (2005) showed that the metallicity of the combined stellar winds remains at a value of $\sim$0.5 $Z_\odot$ from the start of the SB, up to a $t = 3$ Myr evolutionary time, and then rapidly grows to $\sim$15 $Z_\odot$ at $t \approx 7$ Myr, decreasing gradually to $\sim$3 $Z_\odot$ at $t \approx 20$ Myr.

The metal ejection efficiency has two limiting cases: $\xi_z \rightarrow 0$, when all the metallic gas injected by the nuclear starburst is kept in the galaxy disk, and $\xi_z \rightarrow 1$, when all the metallic gas processed in the burst is expelled from the galaxy. Galaxies with $\xi_z \rightarrow 1$ would be metal poor, while the IGM around them should be metal rich. On the other hand, metallic gas injected from the SBs region with $v_g < v_{\rm esc}$ is going to return to the galactic plane, and the ISM of such galaxies will be contaminated with the metals produced in the nuclear starburst.

3.2. *Disk contamination measures*

As mentioned above, bound gas ejected by the SSCs will return to the galactic disk, either close to the center if it never reached a high altitude, or spread to large galactocentric radii if it did. This mechanism is of course a continuum, and "high" or "low" altitude are just relative terms. To quantify the contamination of the disk by material originated in the SSCs we will consider as 'high altitude' a distance of at least 3 times the scale height of the disk, H.

One can define a new parameter, the fraction of bound gas (that is inside a cylinder of radius $R_{\rm max}$ and with velocity less than the escape velocity) that reaches at least an altitude of $3H$:

$$\chi_b \equiv \frac{M_{{\rm ej},3H}}{M_g}\,, \tag{13}$$

TABLE 1

THE GALACTIC MODELS

Galaxy model	M_g $M_\odot$	M_h $M_\odot$	$v_c(r_{200})$ km s^{-1}	H kpc	$N^a_{\rm ep}$	$N^r_{\rm ep}$
G1	6.2×10^6	4.3×10^8	12	0.044	335	478
G2	3.0×10^7	2.1×10^9	20.8	0.071	530	766
G3	7.0×10^7	4.9×10^9	27.7	0.094	473	573
G4	1.4×10^8	9.4×10^9	34.3	0.118	458	646
G5	2.1×10^8	1.4×10^{10}	39.4	0.135	453	681
G6	3.0×10^8	2.1×10^{10}	44.5	0.153	429	666
G7	4.7×10^8	3.2×10^{10}	51.9	0.178	379	655
G8	7.0×10^8	4.8×10^{10}	59.2	0.203	317	585
G9	1.1×10^9	7.3×10^{10}	68	0.233	255	434
G10	1.5×10^{10}	1.1×10^{11}	76.8	0.263	191	317

where $M_{{\rm ej},3H}$ is the total bound mass (including the ISM and the material from the SSCs) that reaches an altitude $\geq 3H$. This mass will be reinserted into the galactic disk at different radii. However, since it includes material both from the SSCs (with high metallicity) and from the ISM around the SSCs (lower metallicity) it is not clear how much the metallicity of the disk will be enhanced by this mixture. For that reason we define the fraction of metallic bound gas that leaves the galactic disk and reaches an altitude between $3H$ and $z_{\rm max}$ as

$$\chi_{b,z} \equiv \frac{M_{c,3H}}{M_c}\,, \tag{14}$$

where $M_{c,3H}$ is the bound mass injected by the stellar cluster that reaches an altitude $3H \leq z \leq z_{\rm max}$, and M_c the total mass injected by the SSC wind. This gives a better measure of the amount of high metallicity material available to spread throughout the disk. Nevertheless, a detailed study of how it will be distributed in the disk is necessary for a complete disk contamination model, which is beyond the scope of this paper.

4. NUMERICAL SIMULATIONS

We have performed adiabatic and radiative 3D N-Body/SPH simulations that model the effect of a central compact starburst, in which mechanical energy is injected by stellar cluster winds, using GADGET-2[3]. All simulations were done with three types of particles: disk, halo, and gas particles, and, unless otherwise stated, each consist of 30000, 40000, and 30000 particles, respectively. Two separate simulations were run for each model, one adiabatic and a second one including radiative losses.

Most simulations (low-resolution simulations) use a timestep $\sim$1–3$\times10^5$ yr and a Plummer softening of 0.25 kpc, 0.5 kpc, and 0.25 kpc, for gas, halo, and disk particles, respectively. We ran a grid of models using different galaxy masses and starburst energies. The parameters of the models are described below.

4.1. *The host galaxies*

We constructed ten isolated galaxies as described in Springel (2000) and in § 2 of this paper. The galaxies are named G1 to G10; they have ISM masses in the range of $\sim 5\times10^6 - 10^{10}\ M_\odot$, similar to those used by MacLow & Ferrara (1999); the total masses are in the $\sim 4\times10^8 - 1\times10^{12}\ M_\odot$ range. The disk masses of the galaxies are given by $M_d = 0.041\ M_{\rm tot}$, and the total mass of the gas is 35% of the galactic visible mass in all of the models.

Table 1 shows the mass of the gas and the halo, the circular velocity at r_{200} and R_0 for all the galactic models.

4.2. *The starburst regions*

In order to reproduce the observed properties of starburst galaxies with young stellar clusters, including M82, NGC 253 and NGC 1569, we use a wide range of SBs masses. We should note that the numbers of these energetic stellar asociations in the host galaxies were detected at optical wavelengths (e.g.,

[3]GADGET-2 is a code for cosmological N-Body/SPH-simulation on serial workstations or massively parallel computers with distributed memory (Springel, Yoshida, & White 2001; Springel 2005).

© Copyright 2011: Instituto de Astronomía, Universidad Nacional Autónoma de México

TABLE 2

THE STARBURST MODELS

Starburst Model	E_c (erg)	$M_{\rm SB}$ ($M_\odot$)
S1	1×10^{52}	$\sim5.5\times10^2$
S2	5×10^{52}	$\sim2.75\times10^3$
S3	1×10^{53}	$\sim5.5\times10^3$
S4	5×10^{53}	$\sim2.75\times10^4$
S5	1×10^{54}	$\sim5.5\times10^4$
S6	5×10^{54}	$\sim2.75\times10^5$
S7	1×10^{55}	$\sim5.5\times10^5$
S8	5×10^{55}	$\sim2.75\times10^6$
S9	1×10^{56}	$\sim5.5\times10^6$
S10	5×10^{56}	$\sim2.75\times10^7$
S11	1×10^{57}	$\sim5.5\times10^7$

for M82 see Melo et al. 2005; for NGC 1569 see Westmoquette et al. 2008). Since there is a high level of obscuration in the nuclear regions of M82, NGC 1569, and NGC 253, the real number of clusters would be larger. Melo et al. (2005) and Smith et al. (2007) have shown that in the nuclear SBs region of M82 the SSCs are confined to the central $\sim$200 pc of the galaxy.

We estimated the mass of the starburst using Starburst 99 models (Leitherer & Heckman 1995 and Leitherer et al. 1999[4]) with the appropriate mechanical energy and a Salpeter initial mass function (IMF) that includes stars between 1 and 100 $M_\odot$. In order to obtain a better estimation of the total starburst masses, we have calculated the mass of the stars between 0.1 and 1 $M_\odot$ using the Kroupa, Tout, & Gilmore (1993) IMF. We assumed that all of the energy produced in the SB lifetime is injected instantaneously, at a given time t_c, inside a spherical region of radius R_c at the center of the disk galaxy as thermal energy. At this time (corresponding to $\sim$10 orbital periods of the galactic disk at a radius of 150 pc), the gas in the central regions of the galaxy has already developed a clumpy structure. Actually, in the present version of the code we cannot consider the case of an injection that extends over a finite time period.

The total injected energy is obtained from

$$E_c = \int_0^{t_f} L_m(t)dt \,, \tag{15}$$

where t_f is the typical SBs lifetime, and $L_m(t)$ the mechanical luminosity as a function of time. The most important contribution to the mechanical luminosity happens at $\sim$40 Myr (see also Leitherer et al. 1999) and after that time the mechanical luminosity decreases drastically, due to the fact that the most massive stars have died by then. Table 2 shows the total energy and the respective mass of all the starburst models (S1–S11).

[4]http://www.stsci.edu/science/starburst99/.

4.3. *The grid of models*

We computed a total of 220 numerical simulations of GWs produced by the nuclear starburst events, with different total masses of the galaxies G1–G10 (see Table 1), combined with different starburst energies S1–S11 (see Table 2), all adiabatic as well radiative (110 models each). The total energy injected by the starburst of the models S1–S11 was distributed in the gas particles inside a sphere of $R_c = 150$ pc at the center of each of the galactic models G1–G10.

We choose this size for the region in which the energy of the starburst is injected, because it is representative of the sizes of observed starbursts. For example, in M82 the starburst region has a $R_c \sim 175$ pc radius (Moorwood 1996), and in NGC 1569A the starburst hole has a $R_c \sim 100$ pc radius (Fujita et al. 2009). An exploration of the effects on our results of varying R_c is shown in § 6.

The number of energetic particles ($N^a_{\rm ep}$ and $N^r_{\rm ep}$, for the adiabatic and radiative cases, respectively) is related to the total number of particles of gas in the initial conditions. The energy per particle in the starburst region is $E_i = E_c/N_{\rm ep}$, the number of energetic points used in the galactic models, is shown in Table 1. All the cluster particles (the energetic particles) are tagged in order to estimate the fate of the metals produced during the starburst lifetime.

5. RESULTS

We have let the galaxy models evolve on their own for $t_c = 1.5 \times 10^7$ yr. At the time t_c, the total energy of the SB is injected in the center of the galaxy. MacLow & Ferrara (1999) injected the energy from the cluster in a continuous way over a period of 40 Myr. Given the fact that the flow induced by the cluster takes $\sim$0.5 Gyr to travel a distance of $\sim$10 kpc (i.e., the size of the galaxy), the differences that might result from releasing the cluster energy over $\sim$40 Myr=0.04 Gyr (rather than instantaneously) cannot be very important.

The ejection efficiencies were computed at $t =$ 1 Gyr in all our models. The values of the efficiencies reach a constant value of integration times of $\sim$0.2–0.5 Gyr and $\sim$0.4–0.7 Gyr for the adiabatic and radiative models (respectively).

© Copyright 2011: Instituto de Astronomía, Universidad Nacional Autónoma de México

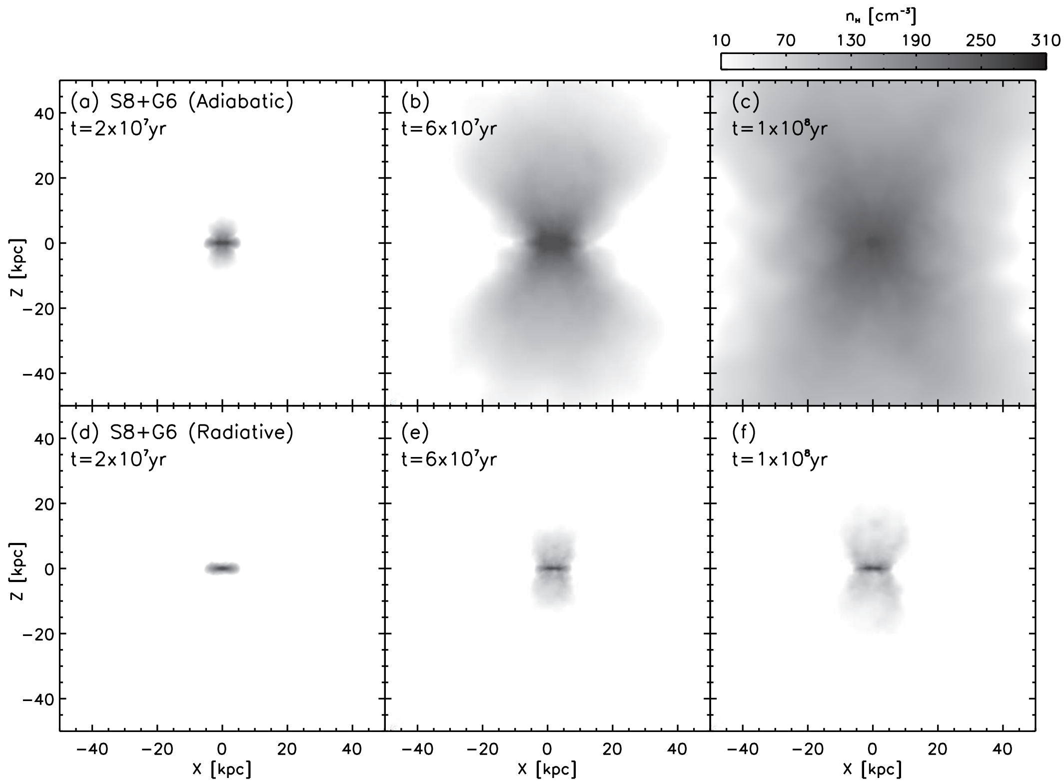

Fig. 1. Time sequence of cuts of number density in the xz-midplane ($y = 0$) for the model S8+G6 (see Tables 1 and 2). The integration times in years are given in the upper left corner of the frames. The top panels (a, b and c) are the adiabatic models, and the bottom panels are the radiative ones.

© Copyright 2011: Instituto de Astronomía, Universidad Nacional Autónoma de México

5.1. *Mass and metal ejection efficiencies*

Total mass and metal ejection efficiencies have been calculated using the definitions given in § 3. In particular, the kinetic and gravitational potential energies as a function of the radial distance r_i (with respect to the center of the potential) were computed for each gas particle. A particle i would escape the galactic gravitational potential if $v_i \geq v_{\rm esc} = \sqrt{-2\Phi_i}$, where v_i is the velocity and Φ_i the total potential at the position of the particle.

We also traced the high metallicity gas particles (injected by the SBs) and the low metallicity gas (galactic ISM gas). The high metallicity gas was tagged with a negative passive scalar, the ISM with a positive one. Therefore, ξ_z was calculated using the gas particles with a negative passive scalar, while ξ_m was calculated with all the gas particles (regardless of the sign of the passive scalar).

Figure 1 shows the temporal evolution of the ejected gas from a central starburst with properties that correspond to starburst model S8 at the center of galaxy model G6 (see Tables 1 and 2). The three timesteps shown are 2×10^7, 6×10^7 and 10^8 yr, for the adiabatic case –panels (a), (b) and (c), respectively–, and the radiative one –(d), (e) and (f), respectively. We can see the ejection of gas from the plane of the dwarf galaxy with a moderate ISM mass ($3 \times 10^8\ M_\odot$), produced by a central starburst that ejects a mass of $1.5 \times 10^6\ M_\odot$. Such a SB corresponds to a region with ~9000 massive stars, injecting a total energy during its lifetime of around 5×10^{55} erg (see the starburst models of Leitherer & Heckman 1995 and Leitherer et al. 1999). From the figure we see right away that the amount of gravitationally unbound gas is larger in the adiabatic than in the radiative case. However, in both cases an important part of the disk gas is pushed above the galactic plane, and in the radiative case a significant part of this gas is returned to the galactic disk.

For this model (S8+G6) the totality of the galaxy gas is pushed above $3H$; however, only 43% of the gas acquires enough energy to leave the galactic potential and become part of the IGM, while the remaining 57% would eventually return to the disk of the galaxy, since this ISM material is gravitationally bound. For the radiative case, the percentage of the

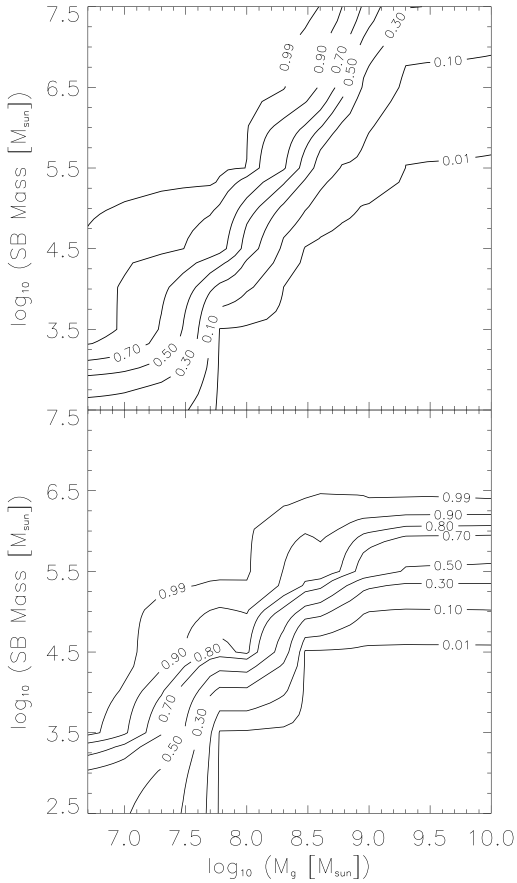

Fig. 2. Mass (ξ_m, top) and metal ejection efficiency (ξ_z, bottom) contours as a function of total mass of the gas and total starburst masses, for adiabatic models (top and bottom panel, respectively).

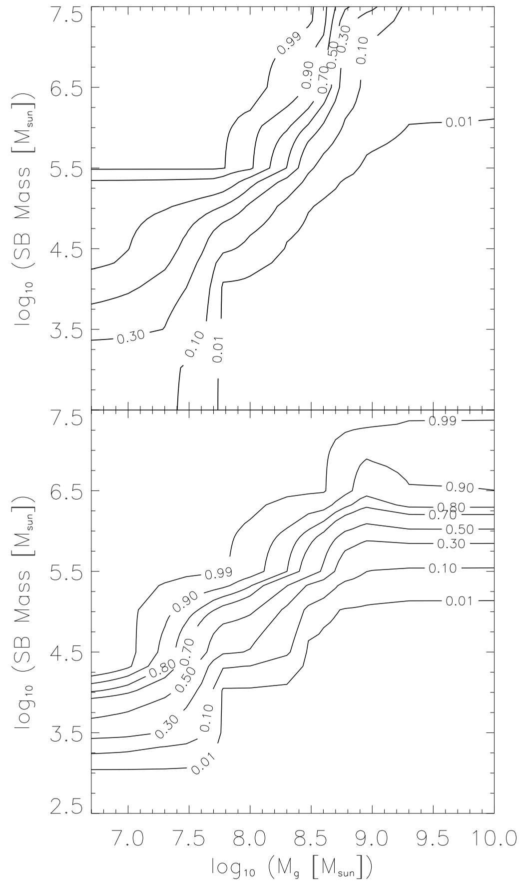

Fig. 3. Same as Figure 2, but for the radiative models.

gas that is gravitationally unbound is of 14%, while 4.7% of the ejected gas gets above $3H$ and returns to the galactic disk. On the other hand, in the adiabatic case 97% of the metallic gas ejected by the nuclear starburst escapes from the galactic gravitational potential. In other words, a galaxy with those parameters would be contaminated only with 5% of the metals produced in the massive SB. For the radiative S8+G6 model, 79% of the metals escape from the galaxy.

The mass ejection efficiencies are presented in Figures 2 and 3, for the adiabatic and the radiative model grids, respectively. In these figures, the abscissa sweeps the galactic models (G1–G10), and the ordinate sweeps the SB models (S1–S11).

Figure 2 shows isocontour maps of the mass ejection efficiency ξ_m (top panel) and the metal ejection efficiency ξ_z (bottom panel) for the adiabatic models as a function of the SB mass and the total gas mass of the galaxy. For the mass ejection efficiency (top panel) we plotted isocontours for $\xi_m = 0.01$, 0.10, 0.3, 0.5, 0.7, 0.9 and 0.99. In this figure, we can see that for the more massive galaxies (in which the gas mass is larger than $10^9\ M_\odot$) the fraction of unbound gas is less than ∼0.25, even for a rather large nuclear starburst. However, galaxies with an ISM of mass lower than $10^8\ M_\odot$ will lose virtually all of their gas if they undergo a nuclear starburst that injects more than $10^5\ M_\odot$.

From the $\xi_z = 0.01$, 0.10, 0.3, 0.5, 0.7, 0.8, 0.9 and 0.99 isocontours in the bottom panel one can see that most of the gas ejected from the cluster escapes the galaxy if the starburst mass is $> 10^{6.5}\ M_\odot$. Also, most of the ejected gas escapes if the galaxy has a total gas mass $< 10^7\ M_\odot$. On the other hand, for starburst masses $< 10^{4.5}\ M_\odot$ and galactic gas masses $> 10^8\ M_\odot$ most of the ejected metals are retained by the galaxy. From the bottom panel of Figure 2 we also see that a starburst with a mass $> 10^{5.5}\ M_\odot$ will eject more than 50% of its wind into the IGM.

© Copyright 2011: Instituto de Astronomía, Universidad Nacional Autónoma de México

© Copyright 2011: Instituto de Astronomía, Universidad Nacional Autónoma de México

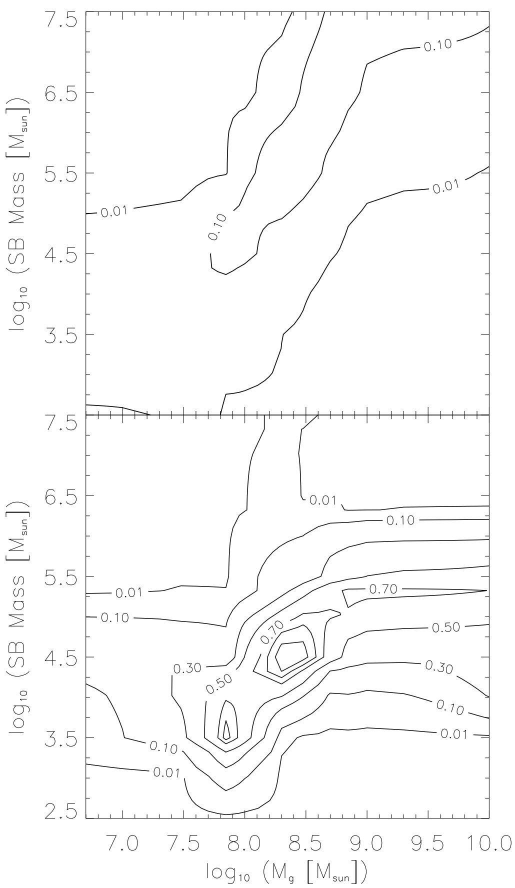

Fig. 4. Fractions of bound gas (χ_b, top) and bound metallic gas ($\chi_{b,z}$, bottom) that reach an altitude of at least $3H$, for the adiabatic models.

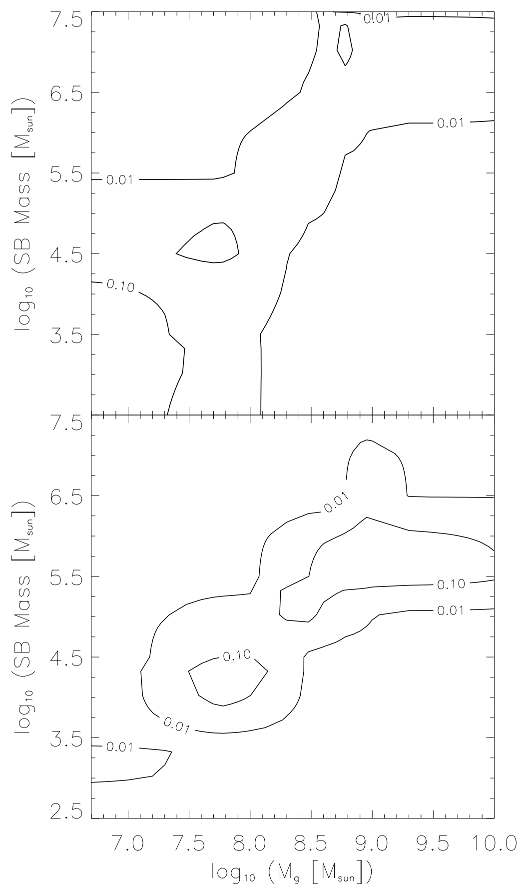

Fig. 5. Same as Figure 4, but for the radiative models.

Figure 3 shows the ξ_m (mass ejection) and ξ_z (metal ejection) efficiencies as a function of galactic gas mass and starburst mass computed from the radiative models. Both the ξ_m and ξ_z contour maps (top and bottom panels of Figure 3) are qualitatively similar to the ones computed from the adiabatic models (see Figure 2). Even though the detailed shapes of the contours vary, the main difference between the radiative and adiabatic cases is the following: in order to obtain similar ejection efficiencies, one needs a starburst mass larger by a factor of $\sim$2 in the radiative case.

5.2. *Material returned to the galactic disk*

Figure 4 shows the efficiencies of gas (χ_b, top panel) and metal mass ($\chi_{b,z}$, bottom panel) which reach at least 3 scale heights (H) above the disk but remain gravitationally bound, computed from the adiabatic models. Both panels show two low efficiency regions divided by a high efficiency ridge (which runs diagonally from low to high SB and galactic gas masses). In the high galactic mass/low SB mass region, the SB ejection mostly remains close to the galactic plane, and does not reach the required $3H$ height above the disk plane (in order to be counted in the χ_b and $\chi_{b,z}$ efficiencies). In the low galactic mass/high SB mass region, the SB ejection mostly escapes from the galaxy. From the $\chi_{b,z}$ distribution (bottom panel), we see that models with $M_g \sim 10^8 \rightarrow 10^9\ M_\odot$ and $M_{\rm SB} \sim 10^3 \rightarrow 10^5\ M_\odot$ are able to redistribute more than $\sim$50% of the ejected metals over the galactic ISM.

Figure 5 shows the χ_b (top panel) and $\chi_{b,z}$ (bottom panel) efficiencies computed from the radiative models. The efficiencies show the same qualitative behaviour (with two low efficiency regions separated by a high efficiency ridge) as the ones calculated from the adiabatic models. However, the maximum values of the efficiencies are lower. In the adiabatic case, the maximum values of the gas mass redistribution efficiency is of $\sim$20%, while a maximum value of only $\sim$10% is found for the radiative models. For the

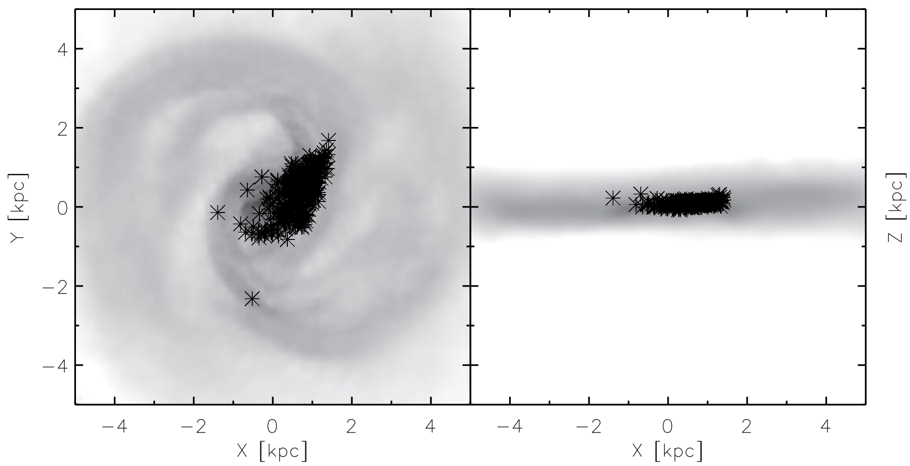

Fig. 6. Distribution of the SPH particles ejected by the central starburst for model S7+G9 after 1 Gyr. The inner region of the domain is shown, and the location of the SPH particles gives the spatial distribution of the metals that have been deposited back on the galactic disk. The left plot shows the distribution of positions projected onto the galactic disk, and the right plot shows the positions of the SPH particles projected onto a plane which includes the rotation axis of the galactic disk. The greyscale shows the distribution of the mass density on these two planes.

metal redistribution efficiency, values above $\sim$70% are obtained for the adiabatic models, while maximum values of only $\sim$20% are obtained from the radiative models.

In Figure 6, we show the distribution of metals that have fallen back onto the galactic disk from the starburst ejection of model S7+G9, after a 1 Gyr time evolution. The SPH particles corresponding to the collapsed material form a distribution with a height of $\sim$300 pc (about the initial scale height of the galactic disk), and with a radial extent of $\sim$2 kpc (see Figure 6), which is about twice the size of the initial scale of length (R_0) of the G9 galaxy (see Table 1). This is an illustration of the fact that in all of our models the infalling metals are redistributed over a large region of the galactic plane.

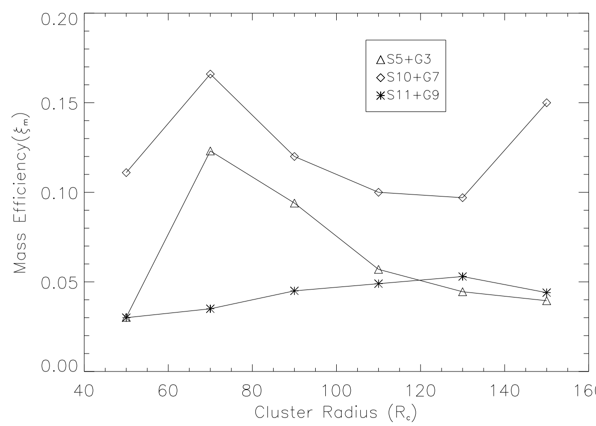

Fig. 7. The mass ejection efficiency ξ_m computed for models S5+G3, S10+G7 and S11+G9 as a function of the initial radius R_c of the starburst.

6. THE EFFECTS OF VARYING THE RADIUS OF THE INJECTION REGION AND THE RESOLUTION OF THE INITIAL STARBURST

In all of the models presented above, we have assumed that the energy from the starburst is injected in a spherical region of radius $R_c = 150$ pc (which is a representative value of the observed sizes of starburst regions, see § 4.3). In this section, we explore the effects on the ejection efficiencies of varying the value of R_c.

We focus on three of the starburst+host galaxy combinations which we have studied above (see Tables 1 and 2). We choose models S5+G3 (a small mass galaxy with an intermediate energy starburst, S10+G7 (an intermediate mass galaxy with a strong starburst) and S11+G9 (a high mass galaxy with a strong starburst). For these three models, we compute radiative simulations in which the starburst energies are injected in spheres of radii $R_c = 50$ to 150 pc (in 20 pc steps). The number of SPH particles within the spheres scales as the volume of the initial starburst (45 particles for $R_c = 50$ pc to 550 particles for $R_c = 150$ pc).

In Figure 7, we show the mass ejection efficiency ξ_m (see equation 11) computed for models S5+G3,

© Copyright 2011: Instituto de Astronomía, Universidad Nacional Autónoma de México

S10+G7 and S11+G9 as a function of the initial radius R_c of the starburst. We see that there is clear dependence of ξ_m on R_c, with differences by factors of $\sim$1.7 (for models S11+G9 and S10+G7), and over $\sim$3.5 for model S5+G3.

We should note that the models with the smaller energy injection regions (with R_c = 50 pc) have smaller mass ejection efficiencies than the models with larger energy injection regions (with R_c = 70 pc, see Figure 7). This is probably due to the fact that in the smaller volumes (covering the denser, inner region of the galaxy) the radiative cooling is stronger. In the models with even larger energy injection regions (with $R_c \geq 90$ pc, see Figure 7), the momentum per unit mass given to the galactic gas is lower, and therefore less material succeeds in escaping from the galactic potential. From these results, we conclude that in our intermediate and high mass galaxy models, variations of factors of $\sim$2 in the efficiencies are to be expected for starbursts (with the same energies) with initial radii in the R_c = 50 to 150 pc range.

We have also explored the effect of changing the total number of SPH particles in the simulations. We again choose models S5+G3, S10+G7 and S11+G9 (see above and Tables 1 and 2) as representative of our model grid, keeping a constant R_c = 150 pc initial radius for the starbursts, and we compute radiative simulations with more than one order of magintud more of gas, halo and disk particles (1500000, 2000000 and 1500000, respectively) than in the previous models (see § 4). In these new runs we have also changed the softening length to 50 pc, for all the components. In all the new models the mass ejection efficiency increases by a factor of the order of 2. For model S5+G3 this change is a factor of $\sim$1.5, while S10+G7 and S11+G9 suffer changes of factors of $\sim$2.21 and $\sim$1.6, respectively.

Therefore, we seem to obtain at least a partial convergence for the values of the ejection efficiencies in simulations with $\sim 10^6$ gas particles. However, the computing time necessary for these simulations is quite large ($\sim$30 times longer than for the 30000 gas particle models), so that our parameter study has been done at lower resolution.

7. DISCUSSION

MacLow & Ferrara (1999) computed radiative, axisymmetric simulations of the ejection of gas from galaxies due to central starbursts. Their models differ from ours in that the starburst energy is injected as a continuous source term during the 50 Myr of their simulations, while in our models the energy of the starburst is injected instantaneously at the beginning of the simulations.

If we convert their starburst mechanical luminosities into total energies (by multiplying the luminosities by 50 Myr), and use the relation between starburst energy and mass of Table 2, we can find correspondences between their models and ours. We then find that both the mass and metal ejection efficiencies computed by MacLow & Ferrara (1999) are generally consistent with the ones that we have computed, with typical differences of factors $\sim$3. We judge this to be a satisfying agreement given the differences between our models and the ones of MacLow & Ferrara (1999).

Interestingly, the highest SB mechanical energy/lower galactic mass model of MacLow & Ferrara (1999) approximately corresponds to our S5+G2 model (with $M_{\rm SB} = 3 \times 10^4\ M_\odot$ and $M_g = 3 \times 10^7\ M_\odot$). As can be seen in Figure 3, this model lies within the transition from low to high efficiency regimes. Therefore, the models of MacLow & Ferrara (1999) mostly missed the transition between low and high mass loss efficiencies which we are describing in the present paper.

D'Ercole & Brighenti (1999) computed a set of 5 models of galaxies with $M_g < 1.4 \times 10^8\ M_\odot$, similar to our galaxy models G1–G5, in which they inject energies in the range of our S6–S8 starbursts. Their "PEXT" model (see Table 2 of D'Ercole & Brighenti 1999) has parameters similar to our S8+G4 model (see Tables 1 and 2). The PEXT model has a $\xi_m = 0.31$ mass ejection efficiency, which is consistent with the $\xi_m = 0.45$ efficiency obtained from our S8+G5 model. D'Ercole & Brighenti (1999) have studied different possibilities (e.g., having galaxies with no rotation, or having fixed dark matter mass distributions) which have not been explored in our present work.

Fragile, Murray, & Lin (2004) computed mass and metal ejection efficiencies produced in galaxies with $10^9\ M_\odot$ (similar to our galaxy model G9) in which they inject energies in the range of our model S3-S7 starbursts. Their model 5 (see Table 1 of Fragile et al. 2004) has parameters similar to our S7+G9 model. Model 5 has a $\xi_m = 0.016$ mass ejection efficiency and $\xi_Z = 0.99$ metal ejection efficiency (see Table 2 of Fragile et al. 2004), which is consistent with the $\xi_m = 0.006$ and $\xi_Z = 0.805$ efficiencies of our model S7+G9. Fragile et al. (2004) have explored the metal ejection efficiencies for supernova events at different radial positions in the galactic disk. They find that a substantial fraction of the metals is retained in their off-center starburst mod-

© Copyright 2011: Instituto de Astronomía, Universidad Nacional Autónoma de México

© Copyright 2011: Instituto de Astronomía, Universidad Nacional Autónoma de México

els. These result shows that if we consider off-center galactic starbursts, the mass and metal ejection efficiencies will be substantially lower than the ones that we have computed in our present paper.

It is worth mentioning that the strong winds produced by the combination of individual stellar winds and SNe explosions not only produce the GWs, but have important consequences on the star formation history of their host galaxy as well. They are the most efficient way to redistribute metals to the ISM (and/or the IGM). This produces a feedback mechanism that facilitates the gravitational collapse of the ISM to form stars. The material with higher metallicity cools more efficiently, and it therefore forms high density condensations on shorter timescales than the metal poor gas (Scannapiecco et al. 2005; Sutherland & Dopita 1993). At the same time, the energy feedback from these strong winds can heat and disrupt cold gas clouds, thus inhibiting star formation.

Observations and theory suggest (e.g., Larson 1974; White & Rees 1978; White & Frenk 1991) that large outflows should be able to develop in small systems because of their shallower potential wells. This is because, according to hierarchical galaxy formation scenarios, large systems are formed by the aggregation of smaller ones. Thus, the energy feedback from strong winds should have a more important effect for systems in the early stages of formation.

Our models provide quantitative predictions of the amount of metals which are ejected into the IGM and which are redistributed within the host galaxy. These predictions could be used in a direct way for computing models of the star formation history of the host galaxy, and could also be included in models of the history of galaxy formation.

8. CONCLUSIONS

We computed 220 numerical simulations of GWs produced by nuclear starburst energy injected inside a spherical region (of radius R_c) at the center of the disk galaxy. We used different total masses of the galaxies G1–G10, combined with different starburst energies S1–S11, all adiabatic as well as radiative (110 models each). We have performed adiabatic and radiative 3D N-Body/SPH simulations of GW models using GADGET-2. The radiative models have been calculated using a solar metallicity cooling function. Finally, the adiabatic models were calculated in order to obtain the maximum possible value of the mass and metal ejection effciency in our models of galactic winds, and do not necessarily correspond to real cases of starbursts in galaxies.

From the grid of models we obtained the mass and metal ejection efficiencies as a function of the mass of the gas in the galaxy and the total mass of the nuclear starburst.

In the same way, we computed the efficiencies of gas and metal mass that reaches at least $3H$ above the disk but remains gravitationally bound for both the adiabatic and radiative regimes. We present these efficiencies as a function of the mass of interstellar medium in the galaxies versus total mass of the nuclear starburst.

We show that for compact starburst regions (e.g., inside the SSC) with masses larger than $10^6\ M_\odot$ in the adiabatic case, the metal injected by the nuclear starburst is expelled to the IGM (at least 90% of this gas). We show that in galaxies with gas masses between 10^7 to $10^{10}\ M_\odot$ and with a massive nuclear starbursts the available metals are freed from the gravitational potential of the galaxy. In the radiative case the critical SB mass at which total loss of metals occurs is around 2 or 3 times larger than in the adiabiatic one.

In addition, we have calculated the efficiency of the metal redistribution in the disk of galaxies. We find that the metal redistribution is more efficient for intermediate and low mass starburst masses ($< 10^{4.5}\ M_\odot$) and galactic gas masses $> 10^8\ M_\odot$ (for both the adiabatic and radiative cases).

In this paper we presented models in which we did not consider many elements that are likely to be important in starburst galaxies; among these are:

- clumpiness in the medium,
- the generation of new stars,
- a different fraction of gas in the galaxy disk,
- the effect of galactic mass loading (see Fujita et al. 2009).

Therefore, there is a large range of possibilities for future studies including differential and/or selective galactic winds (also, Pilyugin 1993 and Recchi et al. 2001, 2002).

Finally, in our paper we have presented a limited resolution study (in § 6). Our evaluation of the dependence of the computed efficiencies on resolution is limited to a range of ∼3 in resolution. This range is of course not very impressive, and questions remain as to the results that would be obtained at considerably higher resolutions (presently not possible, at least for calculating relatively extended grids of models). When such higher resolution models do become available, one will probably find different numerical values for the efficiencies, but one would expect that the transition between low and high ejection efficiency systems (found in the present work) will be preserved.

We thank the anonymous referee for very relevant comments that resulted in a substantial revision of the original version of this paper. We thank Volker Springel (from the Univ. of Heidelberg) for helpful suggestions which we have been included in this paper. We acknowledge support from the Conacyt grants 61547, 101356 and 101975.

REFERENCES

Anders, P., de Grijs, R., Fritze-v. Alvensleben, U., & Bissantz, N. 2004, MNRAS, 347, 17
Cantó, J., Raga, A. C., & Rodríguez, L. F. 2000, ApJ, 536, 896
Chevalier, R. A., & Clegg, A. W. 1985, Nature, 317, 44
Cooper, J. L., Bicknell, G. V., Sutherland, R. S., & Bland-Hawthorn, J. 2008, ApJ, 674, 157
D'Ercole, A., & Brighenti, F. 1999, MNRAS, 309, 941
De Young, D. S., & Heckman, T. M. 1994, ApJ, 431, 598
Fragile, P. C., Murray, S. D., & Lin, D. N. C. 2004, ApJ, 617, 1077
Fujita, A., MacLow, M.-M., Ferrara, A., & Meiksin, A. 2004, ApJ, 613, 159
Fujita, A., Martin, C. L., MacLow, M.-M., New, K. C. B., & Weaver, R. 2009, ApJ, 698, 693
Harris, J., Calzetti, D., Gallagher, J. S., Conselice, C. J., & Smith, D. A. 2001, AJ, 122, 3046
Heckman, T. M., Armus, L., & Miley, G. K. 1990, ApJS, 74, 833
Kroupa, P., Tout, C. A., & Gilmore, G. 1993, MNRAS, 262, 545
Hernquist, L. 1990, ApJ, 356, 359
_________. 1993, ApJ, 409, 548
Larson, R. B. 1974, MNRAS, 169, 229
Leitherer, C., & Heckman, T. M. 1995, ApJS, 96, 9
Leitherer, C., et al. 1999, ApJS, 123, 3
Lynds, C. R., & Sandage, A. R. 1963, ApJ, 137, 1005
MacLow, M. M., & Ferrara, A. 1999, ApJ, 513, 142
Martin, C. L. 1999, ApJ, 513, 156
Melo, V. P. 2005, PhD Thesis, Instituto de Astrofísica de Canarias, Spain
Melo, V. P., Muñoz-Tuñón, C., Maíz-Apellániz, J., & Tenorio-Tagle, G. 2005, ApJ, 619, 270
Meynet, G., & Maeder, A. 2002, A&A, 390, 561
Moorwood, A. F. M. 1996, Space Sci. Rev., 77, 303
Navarro, J. F., Frenk, C. S., & White, S. D. M. 1996, ApJ, 462, 563 (NFW)
Ohyama, Y., et al. 2002, PASJ, 54, 891
Pettini, M., et al. 2001, ApJ, 554, 981
Pilyugin, L. S. 1993, A&A, 277, 42
Recchi, S., Matteucci, F., & D'Ercole, A. 2001, MNRAS, 322, 800
Recchi, S., Matteucci, F., D'Ercole, A., & Tosi, M. 2002, A&A, 384, 799
Recchi, S., Spitoni, E., Matteucci, F., & Lanfranchi, G. A. 2008, A&A, 489, 555
Rodríguez-González, A., Raga, A. C., & Cantó, J. 2009, A&A, 501, 411
Scannapieco, C., Tissera, P. B., White, S. D. M., & Springel, V. 2005, MNRAS, 364, 552
Shopbell, P. L., & Bland-Hawthorn, J. 1998, ApJ, 493, 129
Smith, L. J., et al. 2007, ApJ, 667, 145
Springel, V. 2000, MNRAS, 312, 859
_________. 2005, MNRAS, 364, 1105
Springel, V., Di Matteo, T., & Hernquist, L. 2005, 361, 776
Springel, V., Yoshida, N., & White, S. 2001, New Astron., 6, 79
Strickland, D., & Stevens, S. 2000, MNRAS, 314, 511
Sutherland, R. S., & Dopita, M. A. 1993, ApJS, 88, 253
Tenorio-Tagle, G. 1996, AJ, 111, 1641
Tenorio-Tagle, G., & Muñoz-Tuñón, C. 1998, MNRAS, 293, 299
Tenorio-Tagle, G., Silich, S., & Muñoz-Tuñón, C. 2003, ApJ, 597, 279
Tenorio-Tagle, G., Silich, S., Rodríguez-González, A., & Muñoz-Tuñón, C. 2005, ApJ, 620, 217
Tomisaka, K., & Ikeuchi, S. 1988, ApJ, 330, 695
Veilleux, S., Cecil, G., & Bland-Hawthorn, J. 2005, ARA&A, 43, 769
Westmoquette, M. S., Exter, K. M., Smith, L. J., & Gallagher, J. S. 2007, MNRAS, 381, 894
Westmoquette, M. S., Smith, L. J., & Gallagher, J. S. 2008, MNRAS, 383, 864
White, S. D. M., & Frenk, C. S. 1991, MNRAS, 379, 52
White, S. D. M., & Rees, M. J. 1978, MNRAS, 183, 341

Alejandro Esquivel, Alejandro C. Raga, and Ary Rodríguez-González: Instituto de Ciencias Nucleares, Universidad Nacional Autónoma de México, Apdo. Postal 70-543, 04510 México, D. F., Mexico (esquivel, raga, ary@nucleares.unam.mx).
Pedro Colín: Centro de Radioastronomía y Astrofísica, Universidad Nacional Autónoma de México, Apdo. Postal 3-72, 58090 Morelia, Michoacán, Mexico (p.colin@crya.unam.mx).

© Copyright 2011: Instituto de Astronomía, Universidad Nacional Autónoma de México